

RESEARCH ARTICLE OPEN ACCESS

Bacterial Extracellular Vesicles Exploit Filopodial Surfing and Retraction Mechanisms to Reach the Host Cell Body in an Actin-Dependent Manner

Zia Ur Rehman^{1,2} | Ikenna Obi¹ | Aftab Nadeem³ | Nicole Tegtmeyer⁴ | Steffen Backert⁴ | Anna Arnqvist¹ 

¹Department of Medical Biochemistry and Biophysics, Umeå University, Umeå, Sweden | ²Department of Biotechnology and Genetic Engineering, Kohat University of Science and Technology, KUST, Kohat, Pakistan | ³Department of Molecular Biology, Umeå University, Umeå, Sweden | ⁴Division of Microbiology, Department of Biology, Friedrich-Alexander-Universität Erlangen-Nürnberg, Erlangen, Germany

Correspondence: Anna Arnqvist (anna.arnqvist@umu.se)

Received: 18 April 2024 | **Accepted:** 19 May 2025

Funding: This work was supported by Cancerfonden (22 2382 Pj; 24 3796 Pj), the Foundation for Medical Research at Umeå University and Cancerforskningsfonden i Norrland. The funders had no role in study design, data collection and analysis, decision to publish, or preparation of the manuscript.

Keywords: bacterial extracellular vesicles (BEVs) | extracellular processing | filopodia and cellular extensions

ABSTRACT

Extracellular vesicles derived from gram-negative bacteria are nano-sized particles of different size and origin released by these microbes and are collectively called bacterial extracellular vesicles (BEVs). These BEVs may serve as vehicles for delivering bacterial molecules to eukaryotic host cells. Depending on the bacterial species, BEVs elicit various host cellular and immunomodulatory responses, often aiding bacterial survival and communication. Early events in the initial interaction between BEVs and the host cell, as well as how BEVs reach the cell body, remain unexplored. In this study, we describe the interaction of BEVs with actin-rich cellular extensions, including filopodia and retraction fibres, which extend from the host cell surface. Using microscopy-based tracking at the single cell level, BEVs were shown to exploit cellular extensions at the cell periphery to reach the main cell body, either by hijacking retracted extensions or by surfing along these extensions in an actin-dependent manner. BEVs bind to the outer surface of the extensions, but no internalization occurs at this stage. Instead, they serve as transport for BEVs to the main cell body, where endocytosis takes place. Importantly, this process appears to be a general phenomenon for BEVs across different bacterial species and cell origins.

1 | Introduction

Bacterial extracellular vesicles (BEVs) are released from microbes and play diverse biological roles. In recent years, detailed molecular analyses have significantly advanced our understanding of BEVs, including their chemical composition, biogenesis mechanisms, and biological functions (Schwechheimer and Kuehn 2015; Toyofuku et al. 2019, 2023; Nagakubo et al. 2020). BEVs assist bacteria in disposing of waste materials and acquiring nutrients. They can function as decoys, preventing bacterial destruction,

and serve as carriers of DNA and RNA molecules (Dauros-Singorenko et al. 2018; Bitto et al. 2017). One of their essential functions is acting as delivery vehicles for bacterial components, such as toxins and other host effector molecules, to host cells (Kesty et al. 2004; Wai et al. 2003). Additionally, BEVs play a crucial role in interspecies and intraspecies communication among bacteria (Mashburn and Whiteley 2005).

BEVs are continuously released, with shedding often increasing under stress conditions (Toyofuku et al. 2023; McBroom and

This is an open access article under the terms of the [Creative Commons Attribution-NonCommercial-NoDeriv](https://creativecommons.org/licenses/by-nc-nd/4.0/) License, which permits use and distribution in any medium, provided the original work is properly cited, the use is non-commercial and no modifications or adaptations are made.

© 2025 The Author(s). *Journal of Extracellular Vesicles* published by Wiley Periodicals LLC on behalf of International Society for Extracellular Vesicles.

Kuehn 2007). This is particularly interesting because BEVs act as scavengers, protecting bacteria from threats and enhancing survival (Reyes-Robles et al. 2018; Perez Vidakovics et al. 2010; Park et al. 2021; Lekmeechai et al. 2018). Furthermore, BEVs have been linked to modulating host immune responses, including autophagy, and enhancing antibiotic resistance (Dell'Annunziata et al. 2021; Kaparakis-Liaskos and Ferrero 2015; Irving et al. 2014; Losier et al. 2019; Bitto et al. 2021). BEVs are primarily formed in gram-negative bacteria via blebbing or explosive cell lysis. BEVs generated through blebbing can be classified as outer membrane vesicles (OMVs) or outer-inner membrane vesicles (OIMVs). Biogenesis appears to influence cargo selectivity, as detailed in recent reviews by Toyofuku et al. (2023) and Juodeikis and Carding 2022 (O'Donoghue and Krachler 2016).

Once taken up by host cells, BEVs elicit various host responses, and the pathways involved in their internalization have been a major research focus in recent years (Toyofuku et al. 2023; O'Donoghue and Krachler 2016; Sartorio et al. 2021; Jan 2017; Gan et al. 2023). Some studies suggest that BEVs fuse with the host cell membrane, delivering their contents directly into the host cell cytoplasm (Jäger et al. 2015; Bomberger et al. 2009; Rompikuntal et al. 2012). However, numerous reports describe uptake via endocytic pathways (O'Donoghue and Krachler 2016; Schaar et al. 2011; Olofsson et al. 2014; Turner et al. 2018; Jefferies and Khalid 2020; Guidi et al. 2013; Furuta et al. 2009). Since endocytosis is highly selective based on host cell type, BEV size, and composition, it is unlikely that a single endocytic mechanism applies to all BEVs.

Eukaryotic cells possess actin-rich extensions, including filopodia, retraction fibres, lamellipodia, stereocilia and microvilli. These protrusions serve various functions: filopodia, for instance, facilitate cell migration and environmental sensing. In epithelial cells, filopodia help establish cell-cell contact, guide motility and participate in wound healing, adhesion to the extracellular matrix, neuronal growth-cone pathfinding, endocytosis, and phagocytosis (Yin et al. 2023; Chhabra and Higgs 2007; Mattila and Lappalainen 2008; Ridley 2011; Sanders et al. 2013; Ford et al. 2018). Beyond their direct cellular functions, these protrusions actively capture and process extracellular cargo such as viruses (Schelhaas et al. 2008; Lehmann et al. 2005), bacteria (Romero et al. 2011), exosomes (Heusermann et al. 2016), non-viral vectors (Rehman et al. 2012), and even individual growth factors (Lidke et al. 2005). For example, the gastric pathogen *Helicobacter pylori* (*H. pylori*) interacts with microvilli both in vivo and in vitro (Fiocca et al. 1999; Diesing et al. 2013). More recent research has demonstrated that severe acute respiratory syndrome coronavirus 2 (SARS-CoV-2) hijacks the cilia and microvilli of nasal epithelial cells to penetrate through the mucosal barrier and infect epithelial cells (Wu et al. 2023). Collectively, these findings highlight the role of extracellular extensions in the extracellular processing of various cargoes.

H. pylori infects almost half of the global population, with some individuals developing peptic ulcers or gastric cancer (Malfertheiner et al. 2023). Most *H. pylori* bacteria reside deep within the mucus layer, avoiding the highly acidic gastric lumen, while a smaller population adheres closely to the epithelial cells. BEVs released from *H. pylori* are well-characterized in terms of their chemical composition (Olofsson et al. 2010; Mullaney et al.

2009) and interactions with host cell receptors. Specifically, BEVs surface adhesins, BabA and SabA, bind to ABO/Leb antigens and sLex/a antigens in the gastric epithelium (Olofsson et al. 2010). *H. pylori* BEVs primarily enter host cells via macropinocytosis, clathrin-dependent endocytosis, and caveolin-dependent endocytosis (Olofsson et al. 2014; Turner et al. 2018; Parker et al. 2010). These BEVs carry virulence factors and effector molecules, including the CagA oncoprotein, the VacA cytotoxin, catalase, and HtrA, which induce various host responses upon interaction (Olofsson et al. 2010; Mullaney et al. 2009; Ayala et al. 2006; Ismail et al. 2003). Additionally, non-virulence associated BEV components, such as peptidoglycan, can trigger NOD1-dependent autophagy and inflammatory signalling (Karakis-Liaskos and Ferrero 2015; Irving et al. 2014).

Given that bacteria, viruses and non-viral particles all interact with host cellular protrusions, we aimed to investigate whether these structures play a role in the initial uptake of BEVs by host cells. We used *H. pylori*-derived BEVs and studied their initial binding to gastric epithelial AGS cells. High-resolution imaging revealed that BEVs preferentially bind to actin-rich cellular extensions. Live cell imaging further demonstrated that BEV binding is not random: instead, after attachment, BEVs either 'surf' along the extensions or are actively retracted towards the cell body, where endocytosis occurs. Correlative light and electron microscopy (CLEM) and scanning electron microscopy (SEM) showed that BEVs bind externally to these extensions, with no evidence of endocytosis or fusion occurring along them.

To determine whether this mechanism is unique to *H. pylori*-derived BEVs or if a generalized mechanism exists that applies to different types of BEVs, we also analysed BEVs from *Escherichia coli* (*E. coli*) and *Campylobacter jejuni* (*C. jejuni*). Our findings suggest that the initial BEV-host cell interaction is a general mechanism rather than species-specific. Furthermore, we observed similar behaviours across host cells of different tissue origins, reinforcing the idea that the first contact between BEVs and host cells follows a conserved pathway.

In summary, our findings provide new insights into the extracellular processing of gram-negative BEVs. We propose that BEV processing is a multistep process, beginning when the BEVs attach to and move along cellular extensions before reaching the cell body for internalization. This extracellular processing step occurs before endocytosis, highlighting the complex interactions between BEVs and host cells.

2 | Materials and Methods

2.1 | Cell Culture

Human gastric adenocarcinoma cell line AGS (ATCC1739) was cultured in F-12K nutrient mixture (Thermo Fisher Scientific) supplied with 10% heat inactivated foetal bovine serum (FBS) and 1% penicillin-streptomycin-glutamine supplement (PEST), while HeLa, HEK293 and Caco-2 cells were all grown in Dulbecco's modified Eagle medium (DMEM) F-12 media supplemented with FBS and PEST. All the cells were grown at 37°C and 5% CO₂ and were passaged twice a week. Both PEST and serum were removed during BEVs binding/internalization assays. The

above-mentioned cell culture reagents were obtained from Gibco (Thermo Fisher Scientific). Cell viability was regularly checked in control cells and vesicles treated cells using the trypan blue exclusion test (Strober 2015).

2.2 | Bacterial Strains and Isolation and Purification of BEVs

H. pylori strain P12 (Odenbreit et al. 2002) was grown on Brucella agar plates supplemented with 10% bovine blood (Svenska Labfab, Sweden) and 1% IsoVitox Enrichment (Dalynn Biologicals). The agar was consistently supplied with an antibiotic mixture of Amphotericin B (4 mg/L), Vancomycin (10 mg/L) and Trimethoprim (5 mg/L). *C. jejuni* strain 81–176 was grown in Mueller Hinton agar, and *E. coli* strain MC1061 was grown in Luria broth or Luria agar. Both *H. pylori* and *C. jejuni* were grown in a microaerophilic environment of 5% O₂, 10% CO₂ and 85% N₂, while *E. coli* was grown at 37°C.

2.3 | Isolation of BEVs

BEVs were isolated essentially as previously described (Wai et al. 2003; Olofsson et al. 2010; Sharafutdinov et al. 2024) with the following changes:

For isolation of *H. pylori* BEVs, *H. pylori* strain P12 was exponentially expanded from 1 blood plate to four. Bacteria from 4 agar plates were expanded to 16, and the bacteria from these 16 plates were expanded to 64 plates. Bacteria cultured on the 64 plates were used to inoculate 150 Brucella agar plates (diameter 10 cm). The bacteria were incubated for 48 h and harvested using a sterile disposable 5 mL plastic loop. Bacteria were resuspended in 150 mL of 20 mM Tris-HCl (pH = 8.0) buffer and centrifuged for 30 min at 8000 × g and 4°C. The supernatant was kept and centrifuged once again at 8000 × g.

For isolation of BEVs from *C. jejuni*, strain 81–176 was cultivated according to the above-described procedure on a total of 40 Mueller–Hinton agar plates for 48 h. Bacteria were harvested using a sterile disposable 5 mL plastic loop, resuspended in 100 mL of 20 mM Tris-HCl (pH = 8.0) buffer and centrifuged for 30 min at 8000 × g and 4°C. The supernatant was kept and centrifuged again at 8000 × g.

For isolation of *E. coli* BEVs, 1000 mL of overnight grown *E. coli* MC1061 was centrifuged for 30 min at 8000 × g at 4°C. The supernatant was kept and centrifuged once again at 8000 × g.

The respective supernatant was filtered through a cellulose acetate filter (0.22 mm) and centrifuged for 3 h at 150,000 × g in a precooled centrifuge at 4°C. The supernatant was discarded, and the pellet was resuspended in 20 mM Tris-HCl (pH 8.0). We define this as a crude vesicle extract. The procedure is visualized in a flowchart (Figure 1a, steps 1–3)

2.4 | Purification of BEVs

Purification of BEVs is visualized in a flowchart (Figure 1a, steps 4–7). To purify BEVs in the crude vesicle extract, the

extract was applied to a continuous Histodenz gradient (20–60% Histodenz [Sigma] in 250 mM sucrose/20 mM Tris-HCl [pH 8.0]) and subjected to flotation (Figure 1a, step 5). The sample was loaded in the bottom of the tube using a syringe and separated by equilibrium centrifugation for 16 h at 200,000 × g at 4°C. Typically, 23–24 (500 µL) fractions were collected from top to bottom. The density of each individual fraction was determined using a Brix refractometer. The protein concentration of each individual fraction was determined using Qubit Protein Assay Kits and a Qubit 4 fluorometer (Thermo Fisher Scientific). Two distinct protein peaks were consistently identified: the first peak spanned fractions 3–15, while the second corresponded to fractions 17–24. Although the exact fractions contributing to each peak varied between isolations, the presence of both peaks was a consistent observation (Figure 1b) (Figure 2a in Olofsson et al. 2010). As previously described (Olofsson et al. 2010), purified BEVs were also analysed using transmission electron microscopy (TEM) to confirm that pure BEVs were predominantly present in the first peak (fractions 8–15 in Figure 1b). In contrast, the later peak, fractions 17–24, mainly contained bacterial debris, soluble proteins and lots of flagella (Figure 1c). Fraction 17 contained BEVs and flagellar debris, while fractions 18–23 mainly contained extensive flagellar and cellular debris (Figure 1c). To prepare the TEM grids, BEV samples were applied to formvar-coated copper grids, negatively stained with 1% sodium silicotungstate, and analysed with JEOL1230 transmission electron microscope as previously described (Olofsson et al. 2010).

Fractions containing vesicles (fractions 8–15) (Figure 1c) were pooled and further purified by a fourfold dilution in Milli-Q (MQ) water, followed by ultracentrifugation at 150,000 × g for 60 min at 4°C. The resulting pellet was resuspended in 1 mL sterile 1× PBS buffer (137 mM NaCl, 2.7 mM KCl, 4.3 mM Na₂HPO₄, 1.5 mM KH₂PO₄) and centrifuged at 18700 × g for 20 min at 4°C using a tabletop ultracentrifuge. The supernatant was discarded, and the pellet containing purified BEVs was resuspended in sterile 1× PBS buffer. The purified BEVs were reanalysed by TEM to reconfirm purity (Figure 1d). Size distribution of isolated BEVs and protein concentration were assessed by Nanoparticle Tracking Analysis (NTA) using a NanoSight NS300 instrument (Malvern Panalytical) (Figure 1e). The size distribution of the major BEV population is between 50–200 nm, although some larger BEVs are also observed.

2.5 | Labelling of BEVs

For fluorescent labelling of BEVs, we mainly used the membrane labelling dye FM 4–64FX (Thermo Fisher Scientific), or when needed, immunofluorescence labelling was also used. BEVs (5 µg/mL or stated otherwise) were incubated with the FM 4–64FX dye (5 µg/mL) at either room temperature or on ice for 30 min, followed by two washes in ice-cold PBS. BEVs were resuspended in PBS, and the final protein concentration was measured before adding to cells.

For immunofluorescence labelling of BEVs, antibodies targeting outer membrane proteins were used (Olofsson et al. 2014). Anti-HtrA (1:200) (Zawilak-Pawlik et al. 2019) and anti-BabA (1:200) (Odenbreit et al. 2002) were used as primary antibodies for *H. pylori* BEVs. BEVs were incubated with primary anti-

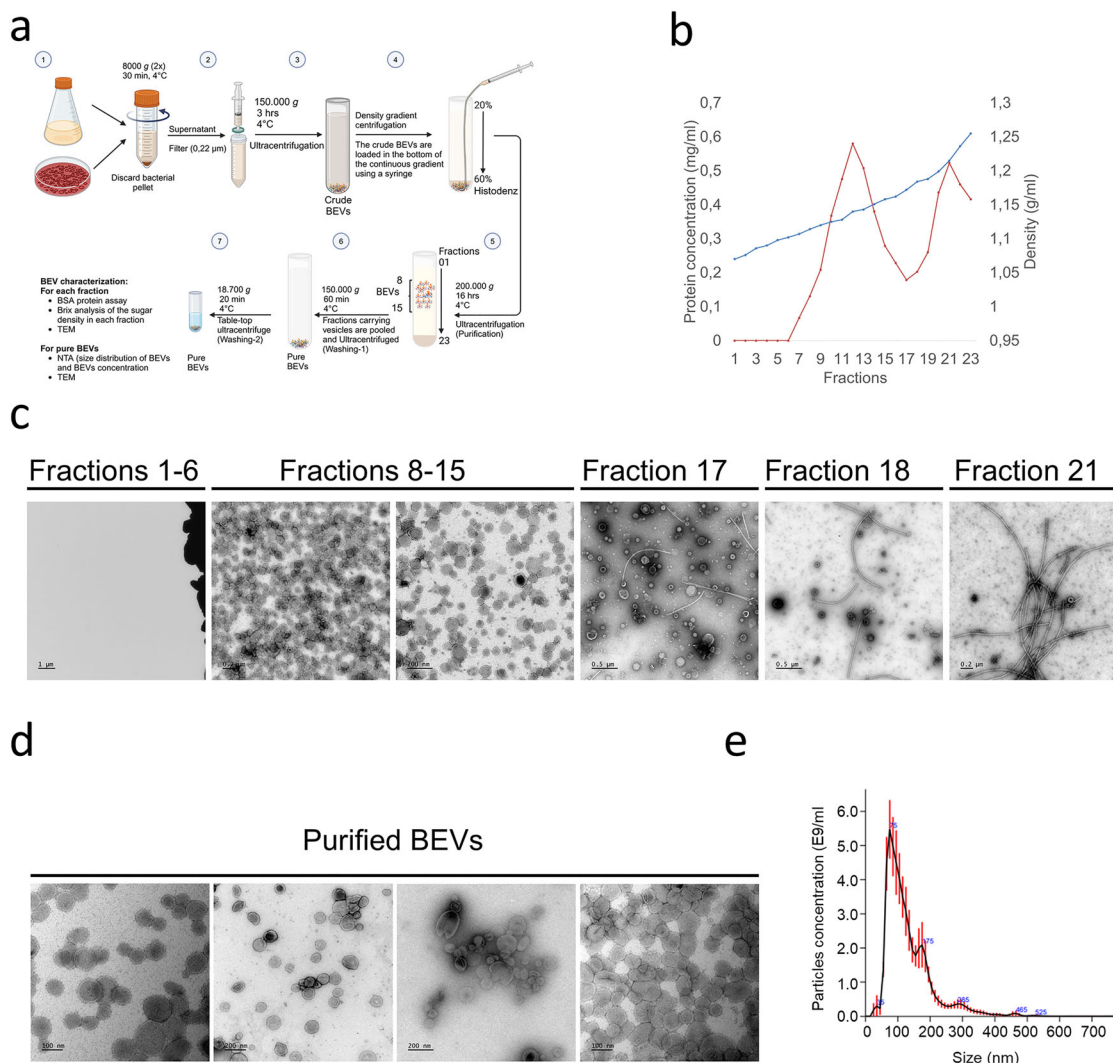


FIGURE 1 | Purity and size of BEVs were confirmed using TEM and NTA. (a) Flowchart illustrating the isolation and purification of BEVs (Created with BioRender); (b) Density (blue) and protein concentration (red) of vesicle fractions measured after crude vesicle purification via density gradient centrifugation; (c) TEM images of various BEV fractions with corresponding scale bars; (d) TEM images of purified BEVs. Scale bars are included in all images; (e) NTA graph showing the concentration and size of purified BEVs. The data are representative of more than ten independent experiments. BEV, bacterial extracellular vesicles; TEM, transmission electron microscopy.

body at room temperature for 1 h, followed by washing in PBS. Alexa-488 conjugated secondary antibody (1:200) (Thermo Fisher Scientific) was used for final labelling of BEVs, incubated for 1 h in the dark at room temperature and then washed 2 times in PBS before adding to cells. As a control, and to check antibody specificity, BEVs were incubated with secondary antibody (1:200) only without prior incubation with primary antibody.

For immunogold labelling of BEVs for visualization in EMs, the same primary antibody was used, but using gold-labelled (5, 10 and 15 nm) protein A as a secondary antibody (1:20). All the primary and secondary antibodies were diluted in PBS containing 1% BSA. All washing steps were done in a pre-cooled Eppendorf 5403 centrifuge at 15000 rpm (23143 × g), 30 min. For the control experiments, only gold-labelled protein A was added to the cells. Cells were further processed similarly for SEM as mentioned above after incubation with BEVs.

2.6 | Plasmid and Transfection

LifeAct-BFP was used for labelling of actin filaments with Lipofectamine2000 (LF2000) as transfection reagent. One day before transfection, cells were plated at a number of 1.5×10^5 /mL and when 60%–70% confluence was reached, cells were transfected following the manufacturer's protocol. Transfected cells were incubated for 24 h for expression of the fluorescent protein. The remaining experiments with BEVs were performed as outlined below.

2.7 | Immunofluorescence Microscopy

Until and unless mentioned, all immunofluorescence experiments were done on live cells or fixed with 4% paraformaldehyde (4% PFA) without permeabilization for subsequent staining. Cells were grown in a glass-bottom 4–8 well chamber slide (μ -slide,

Ibidi) at a confluency of 60%–80%. In order to check the binding of BEVs with cellular extensions, AGS cells were incubated with FM 4–64FX-labelled BEVs for indicated time points in serum free media followed by washing of the cells in PBS two times. Afterwards, 4% PFA also containing Phalloidin-iFluor 488 reagent (ab176753, Abcam) (1:500) was added to cells and incubated for 2 h at room temperature, to fix the cells and for labelling of F-actin filaments at the same time, respectively, without permeabilization. DAPI was used to label the nuclei (Thermo Fisher Scientific). Confocal microscopy was performed using a Nikon A1R Laser Scanning Confocal Microscope supplied with 60× oil immersion lens (Plan Apochromat VC; Nikon, Tokyo, Japan) utilizing NIS-Elements microscope imaging software (Nikon) and a Leica SP8 inverted confocal laser system (Leica Microsystems) equipped with an HC PL APO 63×/1.40 oil immersion lens. Images were further analysed using the ImageJ-Fiji distribution (NIH).

2.8 | Live Cell Imaging

Two days prior to the experiment, cells were plated in glass-bottomed 4-8-well chamber slides (μ -slide, Ibidi), and the next day, cells were transfected with LifeAct-BFP plasmids (as described above). On the day of the actual experiments, cells were directly placed in a temperature-controlled chamber at 37°C with 95% air/5% CO₂ and 100% humidity (Okolab, Ottaviano, Italy). Live cell imaging was performed using either a fully motorized inverted Nikon A1R Laser Scanning Confocal Microscope supplied with 60× oil immersion lens (Plan Apochromat VC; Nikon, Tokyo, Japan) or a Leica SP8 inverted confocal laser system (Leica Microsystems) equipped with an HC PL APO 63×/1.40 oil immersion lens. Cells expressing LifeAct-BFP were selected for imaging prior to the addition of fluorescently labelled BEVs. After the addition of BEVs, image acquisition was directly started using NIS-Element microscope imaging software (Nikon) or LasX (Leica Microsystems). Images were further analysed using the ImageJ-Fiji distribution (NIH). For video sequence analysis we used the Fiji plugin MTrackJ (ImageJ, NIH, USA). The plugin allows manual tracking of individual BEVs giving information about their trajectory, distance travelled, velocity and acceleration. Fluorescence intensity profiles were generated using the plot profile command in Fiji. To count the number of BEVs attached to the cell body and/or internalized, images were converted to ‘RGB color’ followed by the ‘Color threshold’ option in Fiji. Colour intensity was adjusted using the saturation option, and the value of 107 was used for all the images analysed. For inhibitor analysis, cells were pretreated with either 1 μ M Cytochalasin D (CytD), 100 nM Jasplakinolide (Jas) or 10 μ M Nocodazole (Noc) for 30 min before the addition of BEVs.

2.9 | SEM

AGS cells were grown on glass coverslips in 12-well plates (Thermo Scientific, Nunc) at 2×10^5 cells/mL one day before the experiment. Either gold-labelled or unlabelled BEVs were added to cells and incubated for a given time point followed by fixing in 2.5% glutaraldehyde in 0.1 M sodium cacodylate buffer. The samples were dehydrated in a series of graded ethanol, critical point dried and coated with a thin layer of carbon. The samples morphology and BEVs binding were analysed using

field-emission scanning electron microscopy (FESEM; Carl Zeiss Merlin) operating at 4 kV and a probe current of 100 pA. For detection of gold particles attached with BEVs, secondary electron detectors were used.

2.10 | Sample Preparation for SEM/CLEM

AGS cells plated one day before the experiment were incubated with pre-labelled BEVs and incubated for 2 h. To process the sample for SEM/CLEM, cells were fixed in 4% PFA containing phalloidin for labelling of F-actin. We used the ‘shuttle and find’ holder to get the fluorescent images of the cells using a Zeiss Widefield fluorescent microscope (Zeiss, Jena, Germany). Samples were dehydrated in a series of gradient ethanol starting from 70% up to 100% (2 times), followed by critical point drying and finally coated with 1 nm iridium. Images were acquired using field-emission electron microscopy (FESEM; Carl Zeiss Merlin GmbH).

Zeiss Shuttle-and-Find-software that correlates FM and SEM images includes the following steps: (a) mount coverslip on S&F holder; (b) perform calibration (3-fiducials) on FM; (c) capture the FM image; (d) save position for each image; (e) remove coverslip for SEM biological preparation; (f) remount coverslip for SEM imaging; (g) perform calibration (3-fiducials) on SEM; (h) import FM image—go to position with SEM stage; (i) capture SEM image and (j) correlate the FM and SEM images.

2.11 | TEM

In order to observe BEVs under TEM, we used the method as described in Olofsson et al. (2010) and Bäckström et al. (2004). TEM for Figure 3e was performed as follows. AGS cells were incubated with gold-labelled BEVs for a given time point. Subsequently, cells were fixed with 2.5% glutaraldehyde (TAAB Laboratories, Aldermaston, England) in 0.1 M sodium cacodylate buffer, post-fixed in 1% osmium tetroxide, dehydrated with ethanol, a final step in propylene oxide and embedded in Spurr’s resin (TAAB Laboratories, Aldermaston, England). Samples were sectioned 70 nm and picked on Formvar-coated Cu grids and contrasted with uranyl acetate, Reynolds’ lead citrate and finally examined with a JEM1230 transmission electron microscope (JEOL, Söllentuna, Sweden) operating at 80 kV. Micrographs were acquired with a Gatan Orius 830 2k \times 2k CCD camera (Gatan, Abingdon, Great Britain) using Digital Micrograph software.

3 | Results

3.1 | BEVs Bind to Actin-Rich Host Cellular Extensions

The internalization of BEVs to host cells primarily occurs at the main cell body of eukaryotic cells. However, the mechanism by which BEVs reach the cellular surface has not been previously elucidated. Since cellular extensions actively participate in capturing and processing various extracellular cargoes, including viruses, bacteria, exosomes, and non-viral vectors (Schelhaas et al. 2008; Lehmann et al. 2005; Romero et al. 2011; Heusermann

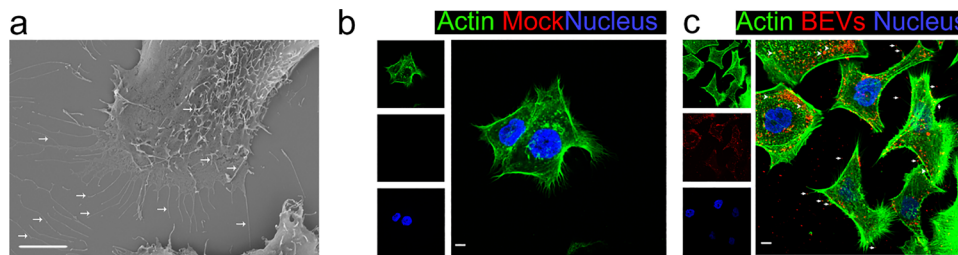


FIGURE 2 | Cells are surrounded by actin rich cellular extensions. (a) SEM image of AGS cells showing cellular extensions (white arrows). Image is a representative of multiple images from three independent experiments; (b) Confocal microscopy image of AGS cells stained with Phalloidin-iFluor 488 (green) to highlight actin and DAPI (blue) to visualize nuclei. A mock control is included. The image represents multiple images from over ten independent experiments; (c) AGS cells incubated with FM 4-64FX-labelled BEVs (red) for 2 h, then stained for F-actin with Phalloidin-iFluor 488 (green) and nuclei with DAPI (blue). BEVs bound to extensions (white arrows) and those on top of the (white arrowheads) are shown. Scale bar = 5 μm . The image is representative of over ten independent experiments. SEM, scanning electron microscopy.

et al. 2016; Rehman et al. 2012), we sought to investigate whether BEVs interact with specific host surface extensions. To address this, we used *H. pylori* BEVs, considering that *H. pylori* is a gastric pathogen, and employed AGS gastric epithelial cells as the host cells. To analyse the presence of extensions around AGS cells, we cultured them on glass coverslips and processed them for SEM and for fluorescent confocal microscopy. SEM analysis revealed cellular extensions ranging in length from 1 to 30 μm , with variable diameters between 50 and 200 nm (Figure 2a, some of the extensions are indicated with arrows). Additionally, SEM confirmed that these extensions were present at the cell surface, indicating that AGS cells are surrounded by these extensions. The size, shape and localization of these protrusions suggested that they correspond to filopodia.

To further assess whether these extensions are rich in structural proteins, particularly filamentous actin (F-actin), we stained AGD cells with Phalloidin. The staining confirmed that these protrusions are indeed actin-rich (Figure 2b). Conversely, tubulin staining was absent in these structures, suggesting that they lack microtubules (Supplementary Data, Figure S1a). In addition to AGS, HeLa cells (human cervical cancer), HEK293 cells (human embryonic kidney) and Caco-2 (human colon carcinoma), exhibit similar protrusions (Supplementary Data, Figures S1a–d)

To examine BEVs interaction with host cell extensions, we incubated AGS cells with FM 4–64FX-labelled *H. pylori* BEVs (red) at 37°C for 2 h. Confocal microscopy revealed BEVs associating with phalloidin stained F-actin filaments (Figure 2c). After prolonged incubation (4 h), BEVs were observed to be associated with cellular extensions (Figure S2a). Additionally, BEVs were observed interacting with these protrusions immediately upon addition to the cells, suggesting a continuous binding process (data not shown). Notably, BEVs also co-localized with actin-rich structures on the apical surface (the top) of the cells (Figure 2c, arrowheads).

3.2 | BEVs Bind to the Outer Surface of the Host Cellular Extensions

In addition to endocytosis, BEVs have also been suggested to fuse with the host cell membrane, releasing their content into the cell cytoplasm (Bomberger et al. 2009; Rompikuntal et al. 2012; Jäger

et al. 2015). Since cellular extensions are actin-rich membrane protrusions, we sought to determine whether BEVs can fuse with these membrane extensions and whether endocytosis can occur at these sites. To investigate this, we employed two imaging techniques: SEM and CLEM.

A key technical challenge was to distinguish BEVs from extracellular vesicles secreted by host cells, as they share structural similarities. To resolve this, we opted to use immunogold-labelling as a tagging method for SEM visualization of BEVs. Specifically, BEVs were labelled with antibodies targeting either the *H. pylori* outer membrane protein BabA or the surface associated serine protein HtrA, followed by gold-conjugated protein A as the secondary antibody. The advantage of pre-labelling BEVs is that it allows for clear differentiation from host-derived extracellular vesicles.

The efficiency of immunogold-labelling of *H. pylori* BEVs was first assessed using TEM. As shown in Figure 3a, BEVs were distinctly labelled with gold particles, confirming the specificity of the labelling (see Figure S2b for additional images). Pre-labelled BEVs were then added to AGS cells and incubated for 2 h before SEM analysis. Again, BEVs were associated with the tips of cell extensions, suggesting a specific interaction (Figures 3b, 3c and Figure S2c for additional images). BEVs are localized not only at the tips and middle sections of these extensions but also near the cell body (Figure 2 and Figure S3c).

In SEM images, bright white dots represent gold labelled BEVs, detected using secondary electron detectors. Unlike conventional immunogold EM, where gold particles appear as black dots, the secondary electron detection method renders them white (Figure 3c, Figure S2c and following figures). As a control, we added only gold-conjugated protein A to the cells, and no free gold particles were observed in the extracellular space or associated with cells (Figure S2d and the magnified inset). Similarly, in BEV-treated cells, no free gold protein A was detected (Figure 3 and Figures S2c and S2e). Additionally, as shown in Figure 2c, BEVs on the cell surface were closely associated with cellular protrusions, further confirming that surface-bound BEVs specifically attach to these extensions (Figure 3f and Figure S2e). While representative images of clustered BEVs are shown for clarity, the same pattern was observed for individual BEVs (Supplementary Materials, Figure S2c [individual BEVs are shown with yellow arrows] and S3a–S3c).

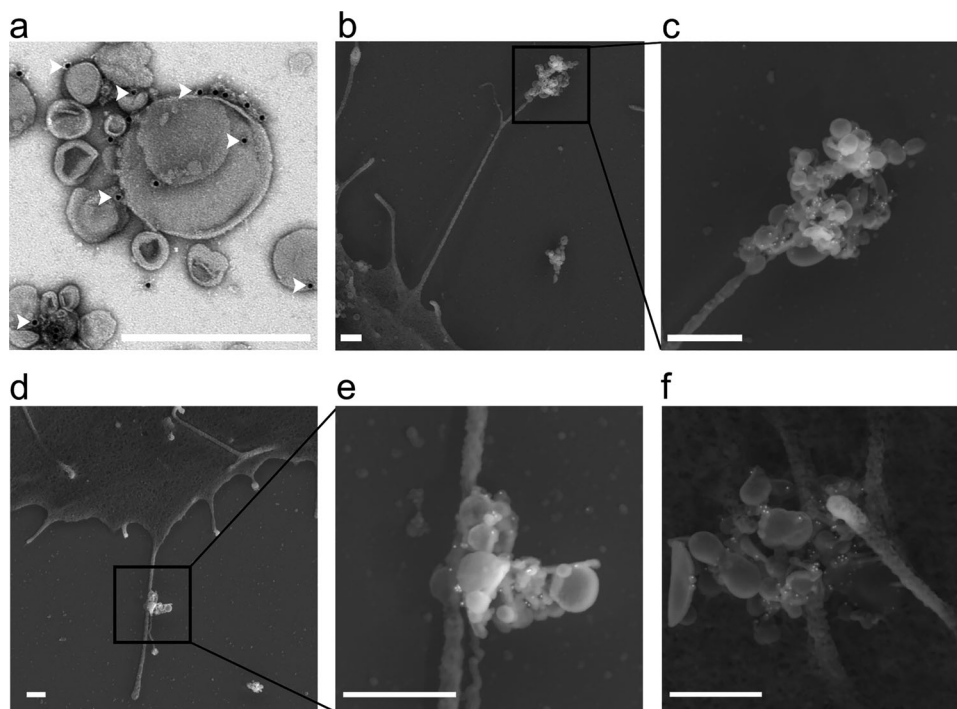


FIGURE 3 | BEVs associate with cellular extensions without endocytosis. (a) TEM analysis of gold-labelled BEVs, with gold particles (arrowheads), confirmed BEVs immunogold-labelling; (b) SEM image showing gold-labelled BEVs bound to cellular extensions; (c) Zoomed-in SEM view confirming BEVs association with cellular extensions; (d) BEVs attached to the mid-sections of extensions; (e) Magnified SEM view further confirming BEV attachment; (f) BEVs observed on top of the cells. White dots indicate the gold-labelled BEVs, confirming their bacterial origin. Scale bars = 0.5 μm . Images represent multiple images obtained from three independent experiments. BEV, bacterial extracellular vesicles; SEM, scanning electron microscopy; TEM, transmission electron microscopy.

Upon incubation with cells, BEVs tended to aggregate, a phenomenon we previously observed (Olofsson et al. 2014). To ensure that individual BEVs were initially added to the cells, we pre-label BEVs with FM4-64FX and examined them using confocal microscopy. Additionally, to confirm the specificity of the antibody and rule out any background signal from the secondary antibody (SAb), we labelled BEVs with Alexa-488-conjugated SAb both in the presence and in the absence of primary antibody (PAb). As shown in Figure S4a, we confirmed that the starting material consisted of individual BEVs and that SAb alone did not produce background signals (Figure S4b). This was further validated by the intensity profile graphs adjacent to each overlay image, demonstrating colocalization in the FM4-64FX condition without PAb (Figures S4a,b). The presence of individual BEVs was also confirmed through NTA analysis, as previously shown in Figure 1e. Thus, these results confirm our previous observation that BEV aggregation occurs after their addition to the cells or possibly when left in culture media for extended periods (Olofsson et al. 2014).

3.3 | CLEM-SEM Confirms That BEVs Bind to the Outer Surface of the Host Cell Extensions

While our previous observations indicated that BEVs attach to cellular protrusions on the apical surface of host cells, we aimed to rule out any potential effects caused by the gold particles used for BEVs labelling. To address this, we examined unlabelled BEVs and observed similar patterns to those seen

with the gold-labelled BEVs (Figure S3c). To further confirm that these vesicles were not host-derived exosomes and to verify that BEVs originated from bacteria while ensuring that gold labelling did not impact their binding, we employed CLEM. CLEM enables the correlation of fluorescence microscopy images with electron microscopy (either TEM or SEM) images, of the same region. Fluorescence microscopy provides a broader view of the sample, and the SEM/TEM image offers more detailed and high-resolution information of the same sample, while SEM/TEM offers high-resolution structural details.

To establish CLEM-SEM analysis for our studies, we first stained F-actin microfilaments using phalloidin-iFluor 488 in combination with a fixative. (Figure 4a). The same cellular regions were imaged using SEM (Figure 4a, SEM). By overlaying fluorescence (actin) and SEM images (Figure 4a, overlay), we successfully confirmed the setup of SEM-CLEM analysis for our experiments.

Next, FM 4-64FX-labelled BEVs were added to AGS cells and incubated for 2 h, followed by actin fibre staining to visualize cellular extensions. A randomly selected cell region was analysed to assess BEVs binding to the extensions. Both SEM and fluorescent microscopy confirmed the presence of BEVs attached to cellular extensions (Figure 4b). A region containing a potential extracellular vesicle (EV) bound to a protrusion (Figure 4b, boxed), was identified in the fluorescent image (inset in the overlay, with an arrowhead indicating a potential BEV). The same region was then imaged at higher magnification using SEM (Figures 4c and 4d).

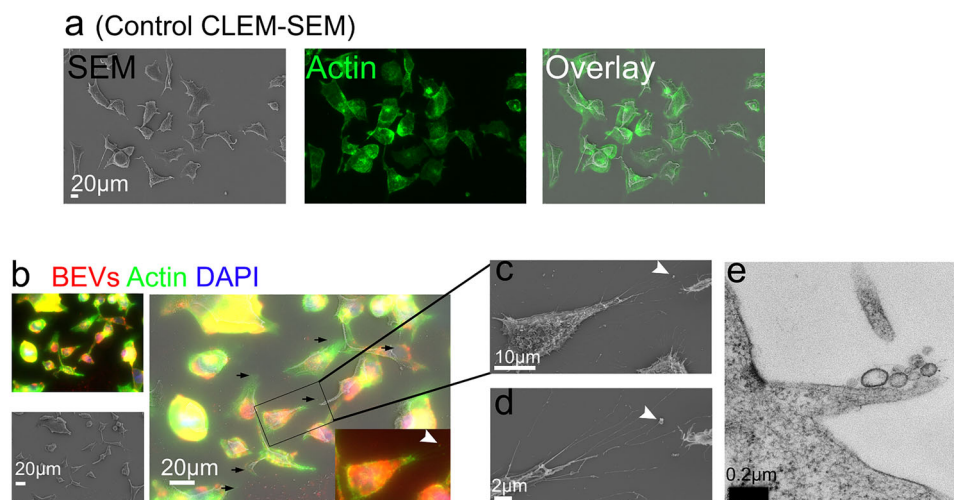


FIGURE 4 | Correlative microscopy further confirms that BEVs are associated with the outer surface of extension. (a) Overlay of SEM and confocal images, demonstrating alignment between different microscopy techniques; (b) SEM image of AGS cells incubated with BEVs. Black arrows indicate BEVs association with extensions. A zoomed-in fluorescent inset highlights a potential BEV (white arrowhead); (c)–(d) SEM images show BEVs on cellular extensions; (e) TEM analysis displays multiple BEVs attached to extensions. Images represent multiple observations from two independent experiments. Scale bars are shown. BEV, bacterial extracellular vesicles; SEM, scanning electron microscopy; TEM, transmission electron microscopy.

Although our findings consistently showed that BEVs attach to the outer surface of cellular extensions, additional control experiments were conducted to further support this conclusion. AGS cells were incubated with gold-labelled BEVs for 2 h, followed by TEM analysis. As shown in Figure 4e, several (Bitto et al. 2017; Kesty et al. 2004; Wai et al. 2003) gold-labelled and unlabelled BEVs were observed binding to the outer surface of cellular extensions, appearing to move to the cell body without internalizing into the extensions (Figure 4e).

Overall, both immunolabelling and CLEM-SEM analysis confirmed that BEVs remained bound to the outer surface of cellular extensions. We did not observe any signs of fusion, endocytosis, or internalization of BEVs into the extensions. Moreover, the widespread binding of BEVs across various regions of the extensions suggests a possible role for these structures in facilitating BEV delivery to the host cell surface.

3.4 | BEVs Are Transported to the Cell Body Via Retractions and Surfing Along Extensions

The observations described above are based on static images. To investigate these interactions in real-time, we complemented our study with live-cell imaging. Since cellular extensions are rich in actin microfilaments, we expressed fluorescently labelled actin (Actin-BFP) in AGS cells (see Materials and Methods for details) and incubated them with fluorescently labelled *H. pylori* BEVs under physiological conditions (i.e., 37°C, 5% CO₂). Actin-BFP expressing cells (pseudocoloured in grey in Fig. 5a) were randomly selected, and live imaging was initiated immediately after BEV addition. Cells that did not express Actin-BFP are outlined with yellow dotted lines in the first frames of Figure 5a. As shown in Figure 5a, three independent BEVs randomly bound to cellular extensions and were subsequently transported to the cell surface (indicated by a line, arrow and arrowhead; see

Supplementary Movie 2). These observations indicate that BEV binding to cellular extensions is a dynamic process.

Beyond retraction, previous studies have shown that various cargos, such as viruses and nanoparticles, can ‘surf’ along filopodia (Schelhaas et al. 2008; Lehmann et al. 2005; Rehman et al. 2012). We investigated whether BEVs exhibit similar behaviour. Indeed, we observed that BEVs initially bound to the tips of extensions and then surfed along them (Figure 5b, Supplementary Movie 3). Notably, the extensions remained stationary; the BEVs actively moved along them, suggesting that these structures function as ‘highways’ for BEV transport (Figure 5b, BEVs are indicated with different coloured arrowheads). Numbers along arrows indicate that four BEVs attached to extensions during the course of imaging. The cell in the top right corner did not express Actin-BFP, and thus no blue fluorescence was observed in that cell (Figure 5b).

To determine whether extensions on the apical surface of cells also process BEVs, we added fluorescently labelled BEVs to LifeAct-BFP-expressing AGS cells. We observed that BEVs initially bound to these extensions, followed by surfing and/or retraction before internalization (Supplementary Movie 4). These findings align with our earlier SEM observations, in which BEVs were detected on top of cellular extensions (Figure 3f and Figure S2e). Furthermore, to rule out any potential impact of fluorescent protein overexpression, we incubated AGS cells with FM4-64FX-labelled BEVs and captured bright-field images of non-transfected cells using live cell imaging (Supplementary Movie 5).

To further analyse BEV dynamics along cellular extensions, we tracked individual BEVs, measuring both their total distance travelled and velocity. Two individual BEVs were tracked over time (Figure 5c; Supplementary Movie 6). The total distance travelled varied depending on the length of the extensions and the initial binding location of the BEVs, whether near the cell body

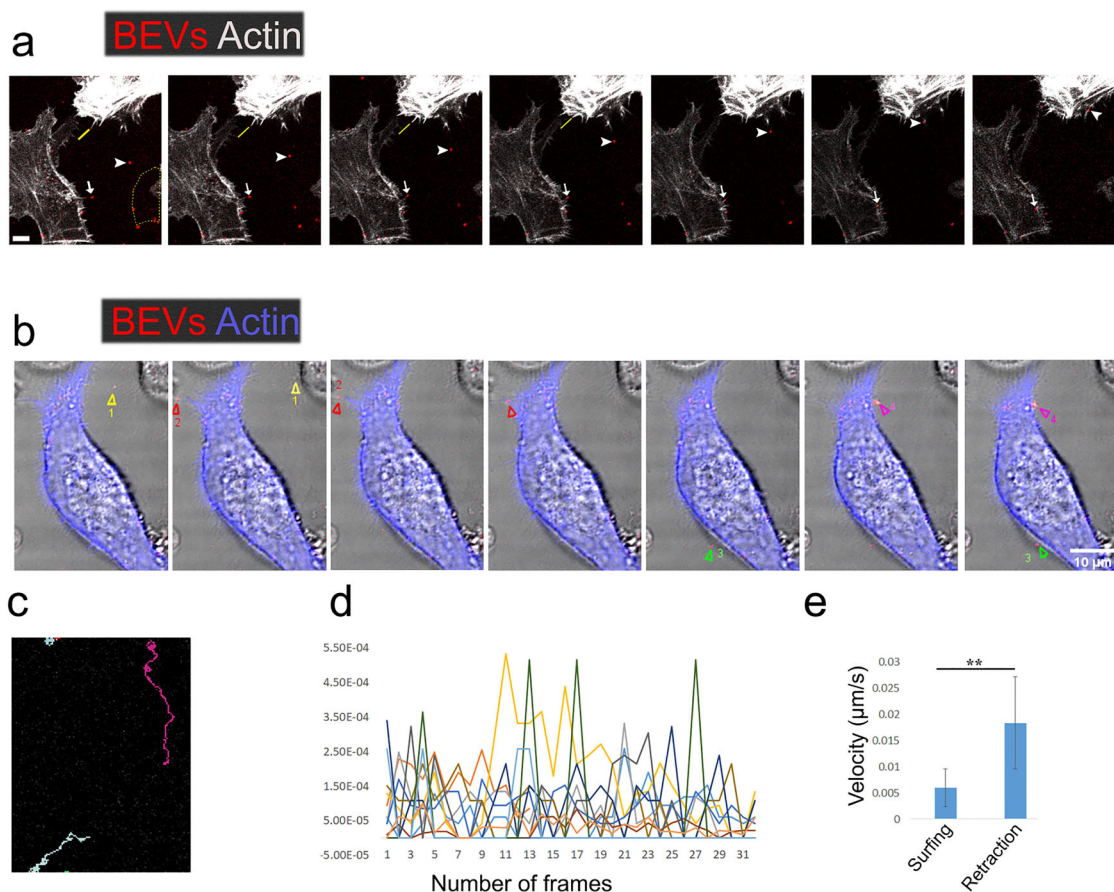


FIGURE 5 | Live cell imaging reveals BEV transport via retraction and surfing. (a) Confocal microscopy of LifeAct-BFP expressing AGS cells (grey) incubated with FM 4-64FX-labelled BEVs (red). Selected frames from [Movie-2](#) (Supplementary Materials) show BEVs reaching cell body via retraction (yellow line, arrow, and arrowhead). Scale bar: 5 μm . For control including only LifeAct-BFP expressing AGS cells, see [Movie-1](#) (Supplementary Materials). (b) Filopodial surfing as a transport mechanism. Selected frames from [Movie-2](#) (Supplementary Materials) show BEVs moving along filopodia towards the cell body. Yellow (1), red (2), green (3) and pink (4) arrows track individual BEVs. Scale bar: 10 μm . Images represent observations from more than ten independent experiments. (c) Trajectories of three BEVs, tracked using the Fiji plug-in in ImageJ (check materials and methods for details), are shown. (d) Individual BEV velocity along extensions varies, sometimes rapid (sliding/collapsing), sometimes stationary ($n = 12$ individual BEVs, selected from 10 independent experiments). Each BEVs was monitored with up to 31 frames until they reached the cell body. (e) Retraction is generally faster than surfing. $n = 30$ observations for each of retractions and surfing, obtained from 10 independent experiments. Error bars show mean \pm SD. $**p \leq 0.01$ (non-parametric two-tailed t -test). BEV, bacterial extracellular vesicles.

or at the tip. Some BEVs attached as close as 1 μm from the cell body, while others were located over 20 μm away. In both cases, the extensions successfully transported the BEVs towards the cell body.

The velocity of BEVs during both surfing and retraction was discontinuous, ranging from an average of 0.001 $\mu\text{m/s}$ (0.06 $\mu\text{m/min}$) to 0.03 $\mu\text{m/s}$ (1.8 $\mu\text{m/min}$). However, during retraction, BEVs occasionally exhibited even higher velocities, reaching up to 0.1 $\mu\text{m/s}$ (6 $\mu\text{m/min}$). Additionally, BEVs sometimes paused during transport, occasionally for extended periods, indicating an irregular, stepwise movement.

Tracking the velocity for 12 individual BEVs over time confirmed this variability (Figure 5d). BEVs were monitored until they reached the cell body (up to 31 frames), and their velocity was measured at each frame (Figure 5d). While both surfing and retraction followed a similar directional movement towards the cell surface, the average velocity of retraction

(0.018 $\mu\text{m/s}$) was notably higher than that of surfing (0.006 $\mu\text{m/s}$) (Figure 5e).

These observations strongly indicate that BEV binding to cellular extensions is not a random occurrence but rather a highly dynamic and specific process. Once bound, BEVs can be transported towards the cell surface via either retraction fibres or by surfing along filopodia.

3.5 | Both Surfing and Retraction of BEVs Along Cellular Extensions Are Actin-Dependent

The retrograde flow of filamentous actin, which facilitates cargo movement along cellular extensions, is driven by actin polymerization at the plus end and/or depolymerization at the opposite minus end (Van Goor et al. 2012; Lin et al. 1996; Burckhardt and Greber 2009). Disrupting either process halts retrograde flow, thereby impairing cargo transport (Figure 6a). Previous studies

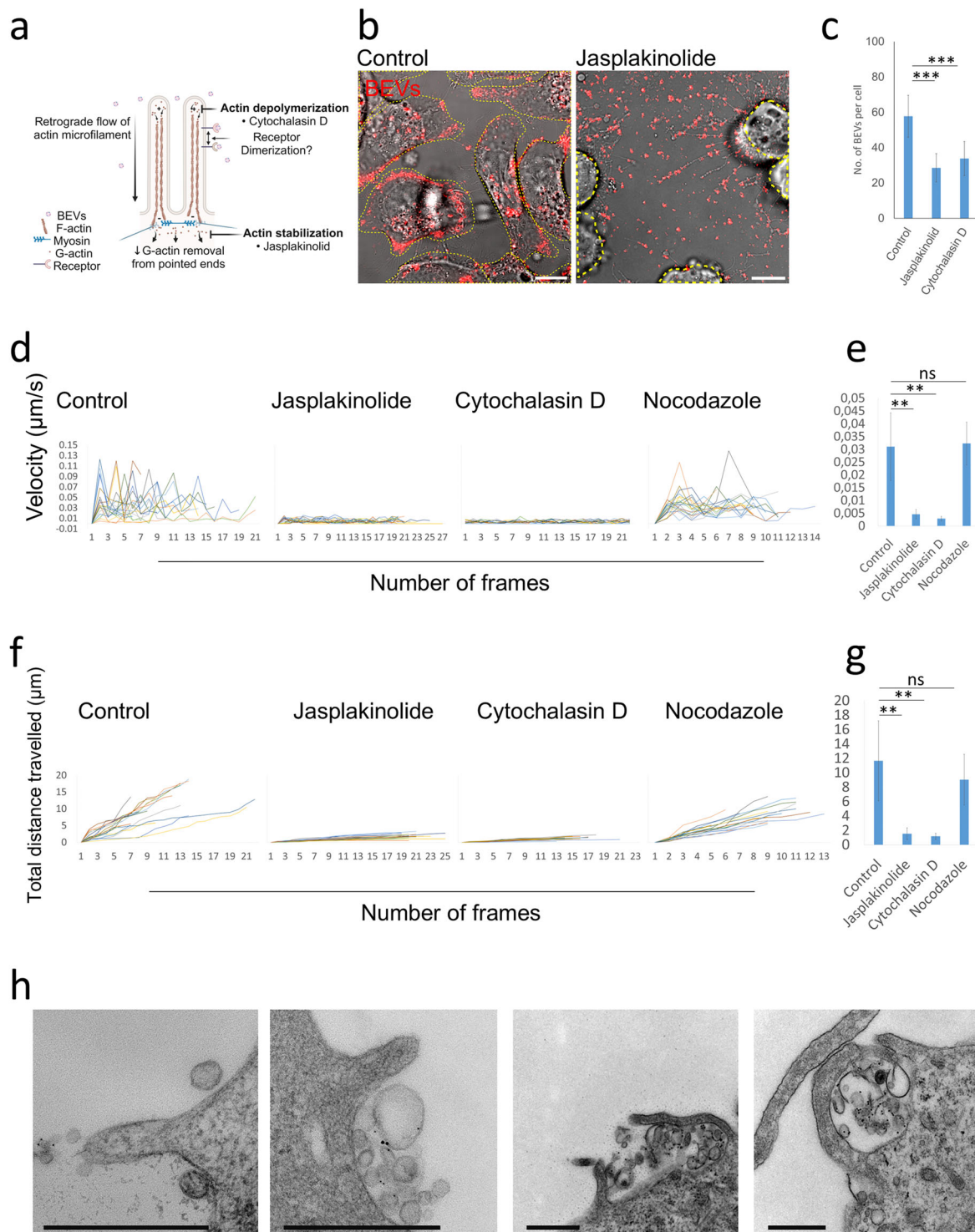


FIGURE 6 | Surfing and retraction movement of BEVs along cellular extensions is actin dependent. (a) Schematic of retrograde flow of actin filament (created with BioRender); (b) Confocal microscopy images of untreated (control) and Jas-treated AGS cells incubated with FM™ 4-64FX labelled BEVs for 2 h. Representative of multiple images from three independent experiments. For a control with only LifeAct-BFP expressing AGS cells, please see [Movie-1](#) (Supplementary Materials). (c) Quantification of BEV association with the cell body in untreated (control), Jas- and CytD-treated cells: 30 cells per condition, three independent experiments. (d) Comparison of BEV velocity in control versus Jas- or CytD- and Noc-treated AGS cells (15 BEVs per condition) from more than 10 independent experiments. (e) Overall average BEV velocity in untreated (control) and treated (Jas, CytD or Noc-treated) cells. (f) Distance travelled by individual BEVs. (g) Average distance travelled by BEVs in untreated and treated cells. The x-axis represents the number of frames counted. (h) TEM images showing endocytosis follows after BEVs move along extensions. AGS cells were incubated with gold-labelled BEVs (10 nm or 5 nm + 10 nm) for 2 h, fixed and analysed via TEM. Scale bar = 0.5 μm . Images represent over 50 observations from four independent experiments. Error bars show mean \pm SD. Two (**) and three (***) asterisks indicate $p \leq 0.01$, $p \leq 0.001$, respectively and “ns” indicates a non-significant difference (non-parametric two-tailed *t*-test).

have demonstrated that actin plays a central role in transporting viruses, bacteria, exosomes and nanocarriers to the cell body for endocytosis (Schelhaas et al. 2008; Lehmann et al. 2005; Romero et al. 2011; Heusermann et al. 2016; Rehman et al. 2012; Burckhardt and Greber 2009).

To investigate the role of actin in BEV transport in more detail, we pretreated AGS cells with either Cytochalasin D (CytD), which depolymerizes actin filaments, or Jasplakinolide (Jas), which stabilizes actin microfilaments (Figure 6a). After a 30-min treatment with CytD or Jas, FM 4–64FX-labelled BEVs were added and incubated for 2-h. In Jas-treated cells, BEVs remained bound to cellular protrusions, but failed to reach the cell body (Figure 6b, dotted outline). In contrast, in untreated control cells, nearly all BEVs successfully reached the cell body, confirming that an intact actin cytoskeleton is essential for BEV transport (Figure 6b, Control). Live-cell imaging further supported this observation, showing that in both CytD- and Jas-treated cells, BEVs remained bound to the protrusions without progressing towards the cell body (Supplementary Movie 7 [Jas] and Movie 8 [CytD]).

Interestingly, in Jas-treated cells, some BEVs detached or moved erratically, suggesting that while binding was not inhibited, the directional movement was lost. To quantify the impact of actin inhibition on BEV access to the cell body, we compared the number of BEVs associated with the cell body between control and inhibitor-treated cells. As shown in Figure 6c, significantly fewer BEVs reached the cell body in CytD- or Jas-treated cells compared to control cells.

The fewer BEVs that were observed in the case of CytD or Jas-treated cells are likely those BEVs that reached the cell body without interacting with filopodia, likely due to direct sedimentation on the cell body. Since distinguishing between sedimented BEVs and those transported via filopodia was challenging, all BEVs associated with the cell body were included in our quantifications.

To further assess the impact of cytoskeletal inhibitors on BEV movement, we measured the velocity of individual BEVs and compared it to controls (Figure 6d). Both CytD and Jas significantly impaired BEV movement, whereas Nocodazole (Noc) (a microtubule-depolymerizing drug) had no effect, confirming that BEV movement is actin dependent and not microtubule dependent (Figures 6d,e). We also determined the overall velocity of all tracked BEVs across the various conditions, which aligned with individual BEV tracking data (Figure 6e), further supporting the conclusion that CytD and Jas inhibit BEVs movement along cellular extensions. Similarly, we compared the distance travelled by individual BEVs (Figure 6f) and assessed whether the total distance travelled was affected by inhibitors (Figure 6g). The numbers indicate the position where BEVs reached the cell body, while the opposite end indicates their initial attachment to the cellular protrusions. Additionally, we tracked BEVs in the untreated (control), CytD-, Jas-treated, and Noc-treated cells (Figure S5). In the presence of both CytD and Jas, BEVs largely remained stationary at their points of attachment to cellular extensions. In contrast, BEVs in control and Noc-treated cells exhibited substantial movement from their attachment point until they reached the cell body (Figure S5).

To investigate whether BEVs internalize into host cells after moving along extensions, we incubated AGS cells with gold protein A-labelled BEVs for 2 h and processed the samples for TEM, as described in the Materials and Methods section. We found BEVs to be endocytosed at the cell body (Figure 6h). Although static images, a series of images demonstrate that BEVs gradually become entrapped within the cellular extensions before being internalized, consistent with our earlier SEM analysis (Figures 3b–d).

3.6 | The *H. pylori* BEVs Surfing and Retraction on Extensions Is a General Phenomenon Across Gram-Negative BEVs and Host Cells

We next investigated whether the observed BEV transport mechanism was exclusive to *H. pylori*-derived BEVs and AGS gastric cells or whether it represents a broader mechanism applicable to BEVs from other gram-negative bacteria and epithelial cells from various tissues. To explore this, we first incubated LifeAct-BFP-expressing HeLa cells with fluorescently labelled *H. pylori* BEVs (Figure 7a). A transport pattern similar to that observed in AGS cells was evident (Supplementary Movie 9). We further tested CHO cells (Figure 7b) and Caco-2 cells (Supplementary Movie 10), which displayed the same BEV transport pattern as AGS and HeLa cells. Additionally, we isolated BEVs from two other gram-negative bacterial species, *E. coli* and *C. jejuni*. Both exhibited a similar behaviour to *H. pylori*-derived BEVs, that is, being transported to the cell body via surfing and retraction of filopodia (Figure 7c and Supplementary Movie 11 and Movie 12, respectively).

Previous studies have shown that *H. pylori* bacteria interact with microvilli both in vivo and in vitro (Fiocca et al. 1999; Diesing et al. 2013). Given the similarities of the surfaces of bacteria and BEVs, we investigated whether *H. pylori* bacteria also exploit cellular extensions for transport. Indeed, when FM4-64FX-labelled wild type *H. pylori* bacteria were added to AGS cells, we observed bacterial movement along extensions towards the cell body (Supplementary Movie 13, arrows).

Together, these findings suggest that BEV surfing and retraction-mediated transport along cellular extensions represent a conserved mechanism across different bacterial species and host cell types.

4 | Discussion

The uptake mechanisms of BEVs by host cells have been extensively studied (O'Donoghue and Krachler 2016; Turner et al. 2018; Jefferies and Khalid 2020; Olofsson et al. 2010; Mullaney et al. 2009). However, the initial contact between BEVs and host cells has remained unexplored until now. In this study, we employed high-resolution imaging techniques to describe, for the first time, the events preceding the initial contact with the endocytosis. We found that BEVs utilize extension surfing and retraction mechanisms to reach the host cell body. Our findings suggest that this mechanism is general and independent of BEVs origin or the type of host cells (Figure 7 and Movies 9–12, Supplementary Materials). Actin-rich cellular extensions, which

resemble highways, play a crucial role in facilitating the transport of various cargos, including bacteria, viruses, exosomes, non-viral vectors, and ligands (Lehmann et al. 2005; Romero et al. 2011; Heusermann et al. 2016; Rehman et al. 2012; Kohler and Rohrbach 2015; Sherer et al. 2007; Young et al. 1992), suggesting that this may be a general mechanism.

Using high-resolution live-cell confocal microscopy, we discovered that BEVs employ both surfing and/or retraction mechanisms to reach the cell body (Figures 3–5). Although, both movements serve the same purpose of delivering BEVs to the cell body, they differ in their underlying cellular mechanisms. Specifically, retraction is regulated by the underlying cytoskeleton, with reorganization driven by polymerization and assisted by molecular motors. In contrast, surfing does not depend on filopodia dynamics, such as displacement or length variation. When we measured the speed of movement, we found that BEV movement was not constant. The average speed during retraction was $0.018 \mu\text{m/s}$, whereas during surfing, it was $0.006 \mu\text{m/s}$ (Figure 5c). These differences in speed are consistent with findings from studies involving other cargo types and their interaction with filopodia (Lehmann et al. 2005; Romero et al. 2011; Heusermann et al. 2016; Rehman et al. 2012).

Using both gold-labelled BEVs and unlabelled BEVs, we did not observe any fusion between the BEVs and the plasma membrane, nor did we detect any internalization at the cellular extensions (Figure 3). Similar observations have been reported for viruses moving along filopodia (Lehmann et al. 2005). Our study utilized both SEM and TEM analysis to investigate these interactions. While SEM is generally sufficient to study BEV fusion with extensions, we also employed TEM due to its successful use in previous related studies (Lehmann et al. 2005). Previous research has suggested that BEVs can fuse with the plasma membrane in lipid raft regions at the cell body (Bomberger et al. 2009; Jäger et al. 2015). However, most rafts and caveolae-associated factors are absent in filopodia, supporting our finding that no fusion occurs between BEVs and the plasma membrane of the extensions (Turner et al. 2018; Jefferies and Khalid 2020; Olofsson et al. 2014). Additionally, we did not observe any BEV internalization at the extensions. This is not surprising, as most endocytic pathways are complex and require multiple factors, which are absent in filopodia (Mattila and Lappalainen 2008; Lehmann et al. 2005; Young et al. 1992).

We did not observe an increase in filopodia formation when BEVs were added to host cells. To gain mechanistic insight into BEVs processing by cellular extensions, we investigate the effects of factors known to be involved in extension formation or retraction by inhibiting the activity. As previously reported, the retrograde flow of actin microfilaments is regulated by actin polymerization and depolymerization (Van Goor et al. 2012; Lin et al. 1996; Burckhardt and Greber 2009). Both CytD and/or Jas have been previously employed to study actin-based motility and cargo movement along filopodia (Lehmann et al. 2005; Romero et al. 2011; Heusermann et al. 2016; Rehman et al. 2012; Lidke et al. 2005). We found that both CytD and Jas inhibited BEVs movement along cellular extensions (Figure 6). Notably, previous studies have shown that Jas prevents receptor oligo- and polymerization (Rehman et al. 2012; Burckhardt and Greber 2009). Our inhibition experiments with Jas confirmed that

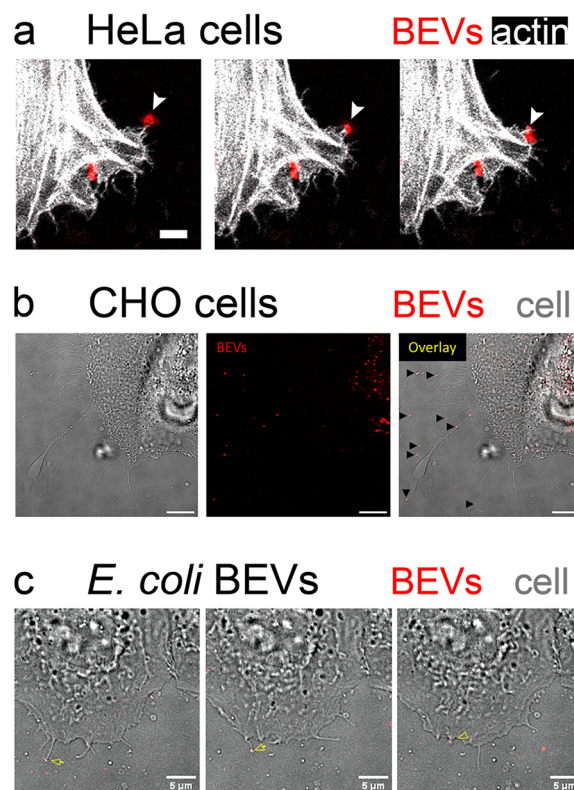


FIGURE 7 | BEV binding and movement along extensions is a general mechanism across cell lines and gram-negative species. (a) Images are from live cell imaging of HeLa cells expressing LifeAct-BFP (grey) incubated with FM 4-64FX-labelled BEVs (red) (Supplementary Movie-8). (b) CHO cells incubated with FM 4-64FX-labelled BEVs (red) for 2 h. BEVs attached to extensions (black arrowheads) are shown in the overlay. Cell body outlined in yellow dotted line (overlay). Scale bar = 10 μm. (c) BEVs derived from *E. coli* (MC1061) exhibit similar attachment and transport mechanism(s), suggesting a conserved process. Data are representative of three independent experiments. Scale bar: 5 μm.

receptors oligo- and polymerization are essential for the efficient trafficking of BEVs to the cell body, where endocytosis takes place.

The cell-lines included in this study were all surrounded by actin-rich cellular extensions (Figures 1a–c and Figure S1). The small Rho GTPase protein Cdc42 has been studied for its role in triggering filopodia formation, and both *C. jejuni* and *H. pylori* have been shown to activate Cdc42 (Churin et al. 2001; Krause-Gruszczynska et al. 2011). Here we observed that *H. pylori* bacteria interact with filopodia. Further studies are needed to specifically follow any increase in formation of filopodia by the bacteria and if such a scenario increases the number of BEVs that are brought to the cell's main body.

Overall, our data provide novel insights into the extracellular processing of BEVs. Our findings enhance the understanding of how BEVs, originating far from cells, are transported to those cells for internalization. Additionally, our results suggest potential mechanisms by which BEVs secreted by bacteria may reach distant cells in vivo. Ongoing studies aim to identify specific host cell receptor(s) involved in the extracellular processing of BEVs.

5 | Conclusions

BEVs utilize cellular extensions to reach the cell surface, either by hitchhiking during retraction or by rolling along the filopodia. The entire process is actin-dependent, and perturbing the actin functions inhibits the movement of BEVs towards the cell body, resulting in decreased access to the cell body and thus fewer that are internalized. Once BEVs have reached the cell surface, internalization into the host cells can occur.

Author Contributions

Anna Arnqvist: conceptualization (equal), data curation (lead), funding acquisition (lead), methodology (equal), project administration (lead), resources (lead), supervision (lead), visualization (supporting), writing – original draft (equal). **Zia ur Rehman:** conceptualization (equal), methodology (equal), software (equal), validation (equal), visualization (lead), writing – original draft (equal). **Ikenna Obi:** methodology (supporting), supervision (supporting), writing – review and editing (supporting). **Aftab Nadeem:** visualization (supporting). **Nicole Tegtmeyer:** methodology (supporting), writing – review and editing (supporting). **Steffen Backert:** methodology (supporting), validation (supporting), writing – review and editing (supporting).

Acknowledgements

We appreciate valuable comments from Prof Richard Lundmark on this manuscript. The authors acknowledge the facilities and technical assistance of Biochemical Imaging Centre at Umeå University (BICU) and the Umeå Core Facility Electron Microscopy (UCEM) at the Chemical Biological Centre (KBC), Umeå University, a part of the National Microscopy Infrastructure NMI (VR-RFI 2016-00968). This work was performed within the Umeå Centre for Microbial Research.

Conflicts of Interest

The authors declare no conflicts of interest.

Data Availability Statement

The data that support the findings of this study are available from the corresponding author upon reasonable request.

References

Ayala, G., L. Torres, M. Espinosa, G. Fierros-Zarate, V. Maldonado, and J. Meléndez-Zajgla. 2006. “External Membrane Vesicles From *Helicobacter Pylori* Induce Apoptosis in Gastric Epithelial Cells: External Membrane Vesicles From *H. Pylori* Induce Apoptosis.” *FEMS Microbiology Letters* 260: 178–185.

Bäckström, A., C. Lundberg, D. Kersulyte, D. E. Berg, T. Borén, and A. Arnqvist. 2004. “Metastability of *Helicobacter Pylori* Bab Adhesin Genes and Dynamics in Lewis B Antigen Binding.” *Proceedings of the National Academy of Sciences* 101: 16923–16928.

Bitto, N. J., R. Chapman, S. Pidot, et al. 2017. “Bacterial Membrane Vesicles Transport Their DNA Cargo Into Host Cells.” *Scientific Reports* 7: 7072.

Bitto, N. J., L. Cheng, E. L. Johnston, et al. 2021. “*Staphylococcus Aureus* Membrane Vesicles Contain Immunostimulatory DNA, RNA and Peptidoglycan That Activate Innate Immune Receptors and Induce Autophagy.” *Journal of Extracellular Vesicles* 10: e12080.

Bomberger, J. M., D. P. MacEachran, B. A. Coutermarsh, S. Ye, G. A. O’Toole, and B. A. Stanton. 2009. “Long-Distance Delivery of Bacterial Virulence Factors by *Pseudomonas aeruginosa* Outer Membrane Vesicles.” *PLoS Pathogens* 5: e1000382.

Burckhardt, C. J., and U. F. Greber. 2009. “Virus Movements on the Plasma Membrane Support Infection and Transmission Between Cells.” *PLoS Pathogens* 5: e1000621.

Chhabra, E. S., and H. N. Higgs. 2007. “The Many Faces of Actin: Matching Assembly Factors With Cellular Structures.” *Nature Cell Biology* 9: 1110–1121.

Churin, Y., E. Kardalidou, T. F. Meyer, and M. Naumann. 2001. “Pathogenicity Island-Dependent Activation of Rho GTPases Rac1 and Cdc42 in *Helicobacter Pylori* Infection.” *Molecular Microbiology* 40: 815–823.

Dauros-Singorenko, P., C. Blenkiron, A. Phillips, and S. Swift. 2018. “The Functional RNA Cargo of Bacterial Membrane Vesicles.” *FEMS Microbiology Letters* 365, no. 5: fny023.

Dell’Annunziata, F., C. Dell’Aversana, N. Doti, et al. 2021. “Outer Membrane Vesicles Derived From *Klebsiella pneumoniae* Are a Driving Force for Horizontal Gene Transfer.” *International Journal of Molecular Sciences* 22: 8732.

Diesing, A., C. Nossol, H. Faber-Zuschratter, et al. 2013. “Rapid Interaction of *Helicobacter Pylori* With Microvilli of the Polar Human Gastric Epithelial Cell Line NCI-N87.” *Anatomical Record* 296: 1800–1805.

Fiocca, R., V. Necchi, P. Sommi, et al. 1999. “Release of *Helicobacter pylori* Vacuolating Cytotoxin by both a Specific Secretion Pathway and Budding of Outer Membrane Vesicles. Uptake of Released Toxin and Vesicles by Gastric Epithelium.” *Journal of Pathology* 188: 220–226.

Ford, C., A. Nans, E. Boucrot, and R. D. Hayward. 2018. “Chlamydia Exploits Filopodial Capture and a Macropinocytosis-Like Pathway for Host Cell Entry.” *PLoS Pathogens* 14: e1007051.

Furuta, N., K. Tsuda, H. Omori, T. Yoshimori, F. Yoshimura, and A. Amano. 2009. “*Porphyromonas Gingivalis* Outer Membrane Vesicles Enter Human Epithelial Cells via an Endocytic Pathway and Are Sorted to Lysosomal Compartments.” *Infection and Immunity* 77: 4187–4196.

Gan, Y., G. Zhao, Z. Wang, X. Zhang, M. X. Wu, and M. Lu. 2023. “Bacterial Membrane Vesicles: Physiological Roles, Infection Immunology, and Applications.” *Advancement of Science* 10: 2301357.

Guidi, R., L. Levi, S. F. Rouf, S. Puiac, M. Rhen, and T. Frisan. 2013. “*Salmonella Enterica* Delivers Its Genotoxin Through Outer Membrane Vesicles Secreted From Infected Cells: Outer Membrane Vesicles and *Salmonella* Genotoxin.” *Cellular Microbiology* 15: 2034–2050.

Heusermann, W., J. Hean, D. Trojer, et al. 2016. “Exosomes Surf on Filopodia to Enter Cells at Endocytic Hot Spots, Traffic Within Endosomes, and Are Targeted to the ER.” *Journal of Cell Biology* 213: 173–184.

Irving, A. T., H. Mimuro, T. A. Kufer, et al. 2014. “The Immune Receptor NOD1 and Kinase RIP2 Interact With Bacterial Peptidoglycan on Early Endosomes to Promote Autophagy and Inflammatory Signaling.” *Cell Host & Microbe* 15: 623–635.

Ismail, S., M. B. Hampton, and J. I. Keenan. 2003. “*Helicobacter pylori* Outer Membrane Vesicles Modulate Proliferation and Interleukin-8 Production by Gastric Epithelial Cells.” *Infection and Immunity* 71: 5670–5675.

Jäger, J., S. Keese, M. Roessle, M. Steinert, and A. B. Schromm. 2015. “Fusion of *L. Egonella Pneumophila* Outer Membrane Vesicles With Eukaryotic Membrane Systems Is a Mechanism to Deliver Pathogen Factors to Host Cell Membranes: Membrane Fusion of *L. Pneumophila* OMVs.” *Cellular Microbiology* 17: 607–620.

Jan, A. T. 2017. “Outer Membrane Vesicles (OMVs) of Gram-Negative Bacteria: A Perspective Update.” *Frontiers in Microbiology* 8: 1053.

Jefferies, D., and S. Khalid. 2020. “To Infect or Not to Infect: Molecular Determinants of Bacterial Outer Membrane Vesicle Internalization by Host Membranes.” *Journal of Molecular Biology* 432: 1251–1264.

Juodeikis, R., and S. R. Carding. 2022. “Outer Membrane Vesicles: Biogenesis, Functions, and Issues.” *Microbiology and Molecular Biology Reviews* 86: e00032–22.

- Kaparakis-Liaskos, M., and R. L. Ferrero. 2015. "Immune Modulation by Bacterial Outer Membrane Vesicles." *Nature Reviews Immunology* 15: 375–387.
- Kesty, N. C., K. M. Mason, M. Reedy, S. E. Miller, and M. J. Kuehn. 2004. "Enterotoxigenic *Escherichia coli* Vesicles Target Toxin Delivery Into Mammalian Cells." *EMBO Journal* 23: 4538–4549.
- Kohler, F., and A. Rohrbach. 2015. "Surfing Along Filopodia: A Particle Transport Revealed by Molecular-Scale Fluctuation Analyses." *Biophysical Journal* 108: 2114–2125.
- Krause-Gruszczynska, M., M. Boehm, M. Rohde, et al. 2011. "The Signaling Pathway of *Campylobacter* Jejuni-Induced Cdc42 Activation: Role of Fibronectin, Integrin Beta1, Tyrosine Kinases and Guanine Exchange Factor Vav2." *Cell Communication and Signaling* 9: 32.
- Lehmann, M. J., N. M. Sherer, C. B. Marks, M. Pypaert, and W. Mothes. 2005. "Actin- and Myosin-Driven Movement of Viruses Along Filopodia Precedes Their Entry Into Cells." *Journal of Cell Biology* 170: 317–325.
- Lekmechai, S., Y.-C. Su, M. Brant, et al. 2018. "Helicobacter Pylori Outer Membrane Vesicles Protect the Pathogen From Reactive Oxygen Species of the Respiratory Burst." *Frontiers in Microbiology* 9: 1837.
- Lidke, D. S., K. A. Lidke, B. Rieger, T. M. Jovin, and D. J. Arndt-Jovin. 2005. "Reaching out for Signals." *Journal of Cell Biology* 170: 619–626.
- Lin, C. H., E. M. Espreafico, M. S. Mooseker, and P. Forscher. 1996. "Myosin Drives Retrograde F-Actin Flow in Neuronal Growth Cones." *Neuron* 16: 769–782.
- Losier, T. T., M. Akuma, O. C. McKee-Muir, et al. 2019. "AMPK Promotes Xenophagy Through Priming of Autophagic Kinases Upon Detection of Bacterial Outer Membrane Vesicles." *Cell Reports* 26: 2150–2165.e5.
- Malferteiner, P., M. C. Camargo, E. El-Oma, et al. 2023. "Helicobacter Pylori Infection." *Nature Reviews Disease Primers* 9: 19.
- Mashburn, L. M., and M. Whiteley. 2005. "Membrane Vesicles Traffic Signals and Facilitate Group Activities in a Prokaryote." *Nature* 437: 422–425.
- Mattila, P. K., and P. Lappalainen. 2008. "Filopodia: Molecular Architecture and Cellular Functions." *Nature Reviews Molecular Cell Biology* 9: 446–454.
- McBroom, A. J., and M. J. Kuehn. 2007. "Release of Outer Membrane Vesicles by Gram-Negative Bacteria Is a Novel Envelope Stress Response." *Molecular Microbiology* 63: 545–558.
- Mullaney, E., P. A. Brown, S. M. Smith, et al. 2009. "Proteomic and Functional Characterization of the Outer Membrane Vesicles From the Gastric Pathogen *Helicobacter pylori*." *PROTEOMICS—Clinical Applications* 3: 785–796.
- Nagakubo, T., N. Nomura, and M. Toyofuku. 2020. "Cracking Open Bacterial Membrane Vesicles." *Frontiers in Microbiology* 10: 3026.
- Odenbreit, S., H. Kavermann, J. Püls, and R. Haas. 2002. "CagA Tyrosine Phosphorylation and Interleukin-8 Induction by *Helicobacter Pylori* Are Independent From AlpAB, HopZ and Bab Group Outer Membrane Proteins." *International Journal of Medical Microbiology* 292: 257–266.
- O'Donoghue, E. J., and A. M. Krachler. 2016. "Mechanisms of Outer Membrane Vesicle Entry Into Host Cells: MicroReview—OMV Entry Into Host Cells." *Cellular Microbiology* 18: 1508–1517.
- Olofsson, A., L. Nygård Skalman, I. Obi, R. Lundmark, and A. Arnqvist. 2014. "Uptake of *Helicobacter Pylori* Vesicles Is Facilitated by Clathrin-Dependent and Clathrin-Independent Endocytic Pathways." *mBio* 5: e00979–14.
- Olofsson, A., A. Vallström, K. Petzold, et al. 2010. "Biochemical and Functional Characterization of *Helicobacter Pylori* Vesicles." *Molecular Microbiology* 77: 1539–1555.
- Park, J., M. Kim, B. Shin, et al. 2021. "A Novel Decoy Strategy for Polymyxin Resistance in *Acinetobacter baumannii*." *eLife* 10: e66988.
- Parker, H., K. Chitcholtan, M. B. Hampton, and J. I. Keenan. 2010. "Uptake of *Helicobacter Pylori* Outer Membrane Vesicles by Gastric Epithelial Cells." *Infection and Immunity* 78: 5054–5061.
- Perez Vidakovics, M. L. A., J. Jendholm, M. Mörgelin, et al. 2010. "B Cell Activation by Outer Membrane Vesicles—A Novel Virulence Mechanism." *PLoS Pathogens* 6: e1000724.
- Rehman, Z. U., K. A. Sjollem, J. Kuipers, D. Hoekstra, and I. S. Zuhorn. 2012. "Nonviral Gene Delivery Vectors Use Syndecan-Dependent Transport Mechanisms in Filopodia to Reach the Cell Surface." *ACS Nano* 6: 7521–7532.
- Reyes-Robles, T., R. S. Dillard, L. S. Cairns, et al. 2018. "Vibrio Cholerae Outer Membrane Vesicles Inhibit Bacteriophage Infection." *Journal of Bacteriology* 200, no. 15: e00792–17.
- Ridley, A. J. 2011. "Life at the Leading Edge." *Cell* 145: 1012–1022.
- Romero, S., G. Grompone, N. Carayol, et al. 2011. "ATP-Mediated Erk1/2 Activation Stimulates Bacterial Capture by Filopodia, Which Precedes Shigella Invasion of Epithelial Cells." *Cell Host & Microbe* 9: 508–519.
- Rompikuntal, P. K., B. Thay, M. K. Khan, et al. 2012. "Perinuclear Localization of Internalized Outer Membrane Vesicles Carrying Active Cytolethal Distending Toxin From *Aggregatibacter Actinomycetemcomitans*." *Infection and Immunity* 80: 31–42.
- Sanders, T. A., E. Llagostera, and M. Barna. 2013. "Specialized Filopodia Direct Long-range Transport of SHH During Vertebrate Tissue Patterning." *Nature* 497: 628–632.
- Sartorio, M. G., E. J. Pardue, M. F. Feldman, and M. F. Haurat. 2021. "Bacterial Outer Membrane Vesicles: From Discovery to Applications." *Annual Review of Microbiology* 75: 609–630.
- Schaar, V., S. P. W. De Vries, M. L. A. Perez Vidakovics, et al. 2011. "Multicomponent *Moraxella Catarrhalis* Outer Membrane Vesicles Induce an Inflammatory Response and Are Internalized by human Epithelial Cells: Characterization of *M. Catarrhalis* OMVs." *Cellular Microbiology* 13: 432–449.
- Schelhaas, M., H. Ewers, M.-L. Rajamäki, P. M. Day, J. T. Schiller, and A. Helenius. 2008. "Human Papillomavirus Type 16 Entry: Retrograde Cell Surface Transport Along Actin-Rich Protrusions." *PLoS Pathogens* 4: e1000148.
- Schwechheimer, C., and M. J. Kuehn. 2015. "Outer-Membrane Vesicles From Gram-Negative Bacteria: Biogenesis and Functions." *Nature Reviews Microbiology* 13: 605–619.
- Sharafutdinov, I., N. Tegtmeyer, M. Rohde, et al. 2024. "Campylobacter Jejuni Surface-Bound Protease HtrA, but Not the Secreted Protease Nor Protease in Shed Membrane Vesicles, Disrupts Epithelial Cell-to-Cell Junctions." *Cells* 13: 224.
- Sherer, N. M., M. J. Lehmann, L. F. Jimenez-Soto, C. Horensavitz, M. Pypaert, and W. Mothes. 2007. "Retroviruses Can Establish Filopodial Bridges for Efficient Cell-to-Cell Transmission." *Nature Cell Biology* 9: 310–315.
- Strober, W. 2015. "Trypan Blue Exclusion Test of Cell Viability." *Current Protocols in Immunology* 111: A3.B.1–A3.B.3.
- Toyofuku, M., N. Nomura, and L. Eberl. 2019. "Types and Origins of Bacterial Membrane Vesicles." *Nature Reviews Microbiology* 17: 13–24.
- Toyofuku, M., S. Schild, M. Kaparakis-Liaskos, and L. Eberl. 2023. "Composition and Functions of Bacterial Membrane Vesicles." *Nature Reviews Microbiology* 21: 415–430.
- Turner, L., N. J. Bitto, D. L. Steer, et al. 2018. "Helicobacter pylori Outer Membrane Vesicle Size Determines Their Mechanisms of Host Cell Entry and Protein Content." *Frontiers in Immunology* 9: 1466.
- Van Goor, D., C. Hyland, A. W. Schaefer, and P. Forscher. 2012. "The Role of Actin Turnover in Retrograde Actin Network Flow in Neuronal Growth Cones." *PLoS ONE* 7: e30959.

Wai, S. N., B. Lindmark, T. Söderblom, et al. 2003. "Vesicle-Mediated Export and Assembly of Pore-Forming Oligomers of the Enterobacterial ClyA Cytotoxin." *Cell* 115: 25–35.

Wu, C.-T., P. V. Lidsky, Y. Xia, et al. 2023. "SARS-CoV-2 Replication in Airway Epithelia Requires Motile Cilia and Microvillar Reprogramming." *Cell* 186: 112–130.e20.

Yin, P., B. J. Davenport, J. J. Wan, et al. 2023. "Chikungunya Virus Cell-to-Cell Transmission Is Mediated by Intercellular Extensions In Vitro and In Vivo." *Nature Microbiology* 8: 1653–1667.

Young, V. B., S. Falkow, and G. K. Schoolnik. 1992. "The Invasin Protein of *Yersinia enterocolitica*: Internalization of Invasin-Bearing Bacteria by Eukaryotic Cells Is Associated With Reorganization of the Cytoskeleton." *Journal of Cell Biology* 116: 197–207.

Zawilak-Pawlik, A., U. Zarzecka, D. Żyła-Uklejewicz, et al. 2019. "Establishment of Serine Protease *htrA* Mutants in *Helicobacter pylori* Is Associated With *secA* Mutations." *Scientific Reports* 9: 11794.

Supporting Information

Additional supporting information can be found online in the Supporting Information section.

Fig. S1: Cellular extensions present in different cell lines are actin rich and are devoid of microtubules. **Fig. S2:** BEV binding to cellular extensions is a frequent and continuous process. **Fig. S3:** BEVs binding to extensions is a continuous process and is independent of BEVs size/clusters **Fig. S4:** FM4-64FX and antibody-based staining confirm that BEVs do not aggregate before incubation with cells. **Fig. S5:** Effect of inhibitors on the total distance travelled by BEVs. MovieS1 jev270107-vid-0002-MovieS1.avi MovieS2 jev270107-vid-0003-MovieS2.avi MovieS3 jev270107-vid-0004-MovieS3.avi MovieS4 jev270107-vid-0005-MovieS4.avi MovieS5 jev270107-vid-0006-MovieS5.avi MovieS6 jev270107-vid-0007-MovieS6.avi MovieS7 jev270107-vid-0008-MovieS7.avi MovieS8 jev270107-vid-0009-MovieS8.avi MovieS9 jev270107-vid-0010-MovieS9.avi MovieS10 jev270107-vid-0011-MovieS10.avi MovieS11 jev270107-vid-0012-MovieS11.avi MovieS12 jev270107-vid-0013-MovieS12.avi MovieS13 jev270107-vid-0014-MovieS13.avi